

New method to search for highly ionizing exotic particles, monopoles, and beyond using time projection chambers

Mesut Arslandok¹,¹ Helen Caines¹,¹ and Marian Ivanov²

¹*Wright Lab, Physics Department, Yale University, New Haven, Connecticut 06520, USA*
²*GSI Helmholtzzentrum für Schwerionenforschung, 64291 Darmstadt, Germany*

 (Received 3 April 2024; accepted 11 July 2024; published 13 August 2024)

Measuring the energy loss and mass of highly ionizing particles predicted by theories from beyond the Standard Model poses considerable challenges to conventional detection techniques. Such particles are predicted to experience energy loss to matter they pass through that exceeds the dynamic range specified for most readout chips, leading to saturation of the detectors' electronics. Consequently, achieving precise energy loss and mass measurements becomes unattainable. We present a new approach to detect such highly ionizing particles using time projection chambers that overcomes this limitation and provides a case study for triggering on magnetic monopoles.

DOI: [10.1103/PhysRevD.110.032013](https://doi.org/10.1103/PhysRevD.110.032013)

I. INTRODUCTION

The discovery of highly ionizing particles (HIP) predicted from theories beyond the Standard Model, such as monopoles, gluinos, Q-balls, strangelets, heavy leptons, etc., would address a number of important questions in modern physics, including potentially the origin and composition of dark matter in the universe and the unification of the fundamental forces [1–4]. While most predictions suggest that such particles are far too massive to be produced in any foreseeable accelerator [5,6], other models suggest a few of these particles, such as magnetic monopoles, could occur in the mass range accessible via the Large Hadron Collider (LHC) at CERN [4,7]. Various technologies and techniques are already being used at the LHC to search for such particles either through tracking detectors by the ATLAS and CMS Collaborations [8–11], or the use of passive detectors, such as the studies underway within the MoEDAL Collaboration [12–18]. However, detecting HIPs, especially in tracking detectors, poses significant challenges. For example, the passage of a HIP through a tracking detector is expected to lead to energy deposits that typically cause saturation of readout electronics, making a positive identification considerably more difficult [19,20].

We propose a novel approach for detecting HIPs that utilizes the continuous readout currently made possible with gas electron multiplier (GEM)-based time projection chambers (TPCs) [21,22] to overcome this saturation effect. Such TPCs are also robust against discharges, even in scenarios with extremely high-energy depositions. In this innovative method, the TPC acts as a passive detector by incorporating an algorithm into the readout electronics that uses the so-called common-mode (CM) signal [23,24]—a

negatively polarized signal below the baseline—as a hardware trigger, followed by offline track reconstruction for HIP identification. The intrinsic design of a GEM-TPC setup offers other distinct advantages, such as a low material budget, compared to solid-state tracking detectors, and an extensive 3D tracking volume.

This report is organized as follows. In Sec. II we give a brief introduction to TPCs and provide more details on the common-mode effect. In Sec. III, as an example of our proposed HIP identification technique, we conduct an in-depth case study on potential energy loss measurements of magnetic monopoles using the GEM-based TPC that is currently in operation at the ALICE experiment at the LHC [25,26]. Finally, we conclude in Sec. IV with a discussion on how the proposed approach can be employed for more general HIP identification.

II. GEM-BASED TPCS, THE COMMON-MODE EFFECT, AND ALICE'S TPC

TPCs [22,27–29] are typically built as large gas-filled cylindrical or box-shaped chambers. Examples of TPCs in current use in nuclear physics heavy-ion experiments include NA61 [30] at the SPS, STAR [31,32] and sPHENIX [33] at RHIC, and ALICE [23,34] at the LHC. Equipped with an array of sensitive detectors (e.g., MWPCs and GEMs), TPCs capture the ionization signals generated by charged particles passing through the gas. As particles move through the gas, they ionize the atoms or molecules along their path, generating ionization electrons and positively charged ions. The electrons are collected at a readout plane via an electric field that is applied across the gas volume. An additional large electric field at the MWPC or GEM readout plane creates an

electron avalanche leading to a significant increase in the number of electron-ion pairs and thus the signal amplitude. The arrival points in the readout plane provide the x and y coordinates, while the drift time is used to determine the z -coordinate of the initial ionization point. In this way, TPCs enable reconstruction of the trajectories of charged particles in three dimensions. The typical resolution along the time axis (z) is coarser than solid-state trackers, being typically on the order of several hundred microns compared to ten microns. However, TPCs benefit from their low material budget and abundance of ionization points, enabling segmentation of the x - y plane into many more samples as compared to solid trackers. This capability allows for the detection of long tracks and effective use in large volumes, making TPCs well-suited to high-track density environments. In addition, the ability to control the amplification enables energy loss measurements of HIPs.

The primary challenge for TPCs is posed by the ions generated during both primary ionization and the subsequent gas amplification. These ions induce a so-called space charge effect, which distorts the electric field within the gas volume and influences the trajectory of subsequent primary ionization electrons. The amount of ions produced during gas amplification far exceeds that of primary ionization, so TPCs are designed to prevent as many ions as possible from entering the drift volume. Multiwire proportional chambers (MWPCs) [22] employ gating wires for this purpose. These wires are positioned as the outermost wire layers and operate in two modes: open and closed. In open gate mode, all wires of the gating grid are kept at a common potential so that the grid is transparent to charge transport between amplification and drift regions. In closed mode, on the other hand, the ions are blocked with alternating voltages, resulting in an ion leakage into the drift region of less than a factor of 10^{-4} [34]. The gating grid is closed by default and only opened in case of an event trigger. This opening and closing of the gating wires imposes limitations on TPC readout speeds. In contrast, GEMs [21,22] inherently block ions from reentering the drift region without the need for a gating grid, albeit with a higher rate of ion leakage. In the ALICE TPC, for example, an ion leakage of about 0.7% was achieved by optimizing the voltage settings and hole sizes of the GEM foils [23]. The continuous readout operation mode of GEM-based TPCs enables the measurement of very long signal tails, caused for example by the significant energy depositions expected from HIPs—a capability we will further discuss below in the context of the ALICE TPC.

The ALICE TPC, which is operated in a 0.5 T solenoidal magnetic field parallel to its axis, is the main tracking and particle identification (PID) detector in the central barrel of the ALICE experiment [23,34,35]. The TPC consists of a large cylindrical vessel, with a total active volume of 88 m^3 , filled with a Ne-CO₂-N₂ (90-10-5) gas mixture

(i.e., 90 parts of Ne, 10 parts of CO₂, and 5 parts of N₂) [23]. It is divided equally into two drift regions by a negatively charged central membrane at its axial center. The TPC sectors, each covering 20° in azimuth, are located at the ends of the drift volume. They are radially segmented into inner and outer readout chambers (18 IROC and 18 OROC on each side respectively). A uniform electric field along the z -axis is generated by the field cage.

The anode plane of the readout chambers comprises a total of 524,160 pads, which are arranged in 152 rows in the radial direction. The number of pad rows determines the largest possible number of hit points—so-called clusters, concentrated charge deposits that are detected within a search window extending over three bins in the pad-row direction and three bins in the time direction—along the trajectory of a given particle. Each pad is connected to a front-end electronics channel with 160 front-end channels combined in each front-end card. More details about the TPC and its performance can be found in Refs. [23,34].

The ALICE TPC was upgraded from MWPC-based readout to GEM-based readout during the second long shutdown (December 2018–March 2022) of the LHC. This upgrade was necessary to cope with the predicted minimum bias Pb-Pb collision rate of 50 kHz during the Run 3 and Run 4 (2022–2030) data acquisition periods [23,36,37]. To achieve the required gain while effectively suppressing the back-flow of ions produced during the amplification stage, a quadruple GEM configuration was chosen. A TPC sector is divided into four GEM stacks; one for IROC and three for OROC (see Fig. 4) in the radial direction. The main components of the mechanical structure of the readout chambers consist of a trapezoidal aluminum frame (Al-body), a pad plane separated from the Al-body by a fiberglass plate (strongback), and a stack of four GEM foils, more details of the structure of an IROC are shown in Fig. 6 of [23].

Within the GEM readout system, the pad plane, and the GEM foils possess an inherent capacitance that leads to the so-called common-mode effect [24]. It is created by their common high-voltage supply via a resistor network. An illustration of the common-mode effect is shown in Fig. 1. When a signal is detected on a single pad (S), a capacitive signal with opposite polarity is induced across all pads facing the corresponding stack ($s_1 \dots s_n$) so that the total positive charge is proportional to the total negative charge, $Q_{\text{tot}}^+ = k_{\text{CF}} \times Q_{\text{tot}}^-$ at a given time. The factor k_{CF} depends mainly on the stack size (see Table 2 of Ref. [24]). Consequently, the amplitude of the common-mode signal in a given pad is suppressed by a factor of N_{pads} relative to the total positive charge, where N_{pads} is the number of pads belonging to the same stack. It is worth noting that a similar common-mode effect is observed in the MWPC-based ALICE TPC [38].

A typical semi-Gaussian TPC signal together with the simultaneous common-mode signal seen as an undershoot

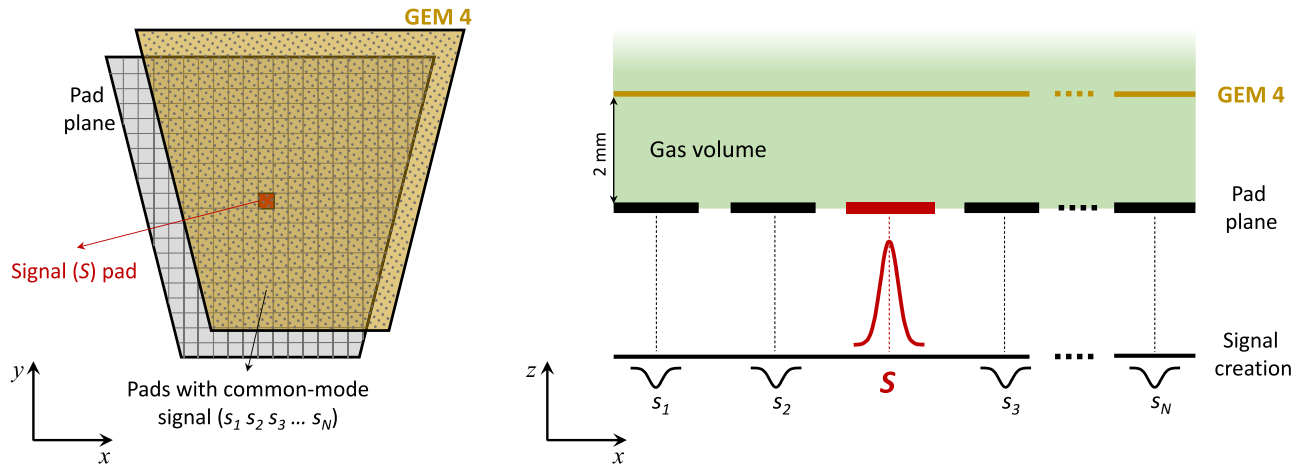


FIG. 1. Illustration of the common-mode effect. Left: The $x - y$ projection of pad plane and the GEM foil closest to the pad plane (GEM 4), with the pad displaying a signal (S) highlighted in red and those showing the common mode signal (s_i , $i = 1, 2, 3 \dots N = N_{\text{pads}}$ and $\sum_{i=1}^{N_{\text{pads}}} |s_i| = S$ in the case of perfect charge conservation) depicted in gray. Right: The corresponding $z - y$ projection illustrates a signal (red) and the resulting negatively polarized common-mode signals (black) at a given time, where z is the drift direction of the electrons and the gas volume is represented by a green shaded area. These are simple sketches and not drawn to scale.

in the neighboring pads, is shown in Fig. 2. Under real experimental conditions, the common-mode effect results in an average baseline drop and an effective noise contribution, as illustrated via simulation in Fig. 3. At the highest expected occupancy during Run 3 and Run 4, the average baseline shift of the ALICE GEM-based readout is about 3 ADC counts, compared to an average signal peak height of about 80 ADC counts. As detailed in [24], an online correction algorithm that measures the common-mode signal has already been implemented in the FPGA-based readout electronics of the ALICE TPC.

In the following, we discuss the expected response of the ALICE TPC in the presence of an energy deposit equivalent to that of a monopole. We show that the amplitude of the

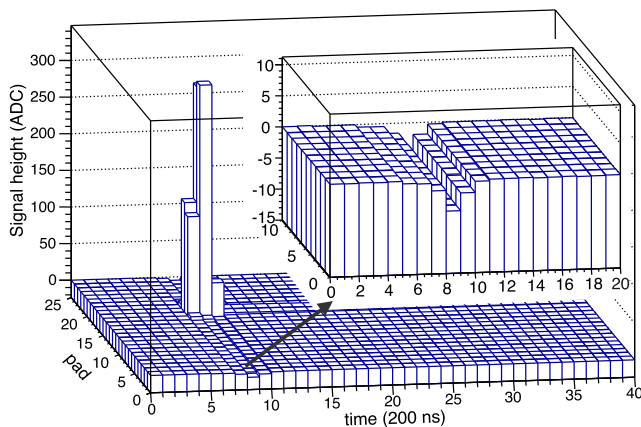


FIG. 2. The main figure shows the ADC signal after pedestal subtraction and before zero suppression for a hit in an ALICE GEM-TPC sector, the inset shows the common-mode effect measured at the same time along the other pads. Figure taken from [23].

baseline drop is expected to be much larger providing inspiration for use as a monopole or any other HIP trigger.

III. HIP IDENTIFICATION: A CASE STUDY ON MONOPOLES

When a relativistic monopole [5] possesses a single Dirac charge and is in motion, its energy loss due to ionization is equivalent to that of a relativistic particle

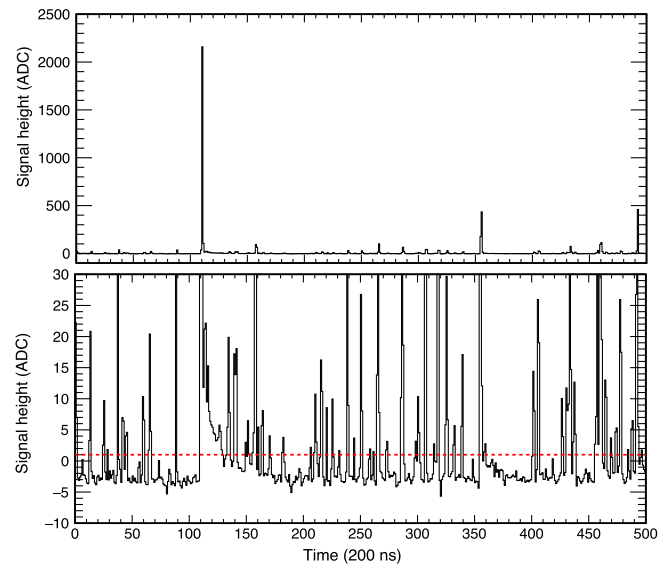


FIG. 3. Simulation of a pad signal for an event with $\approx 30\%$ occupancy, representing the highest expected track density in the ALICE TPC in Run 3. Top: Full signals are shown. Bottom: A zoom-in on the y -axis to reveal the baseline fluctuations, the red-dashed line shows the zero-suppression threshold. Figure taken from [24].

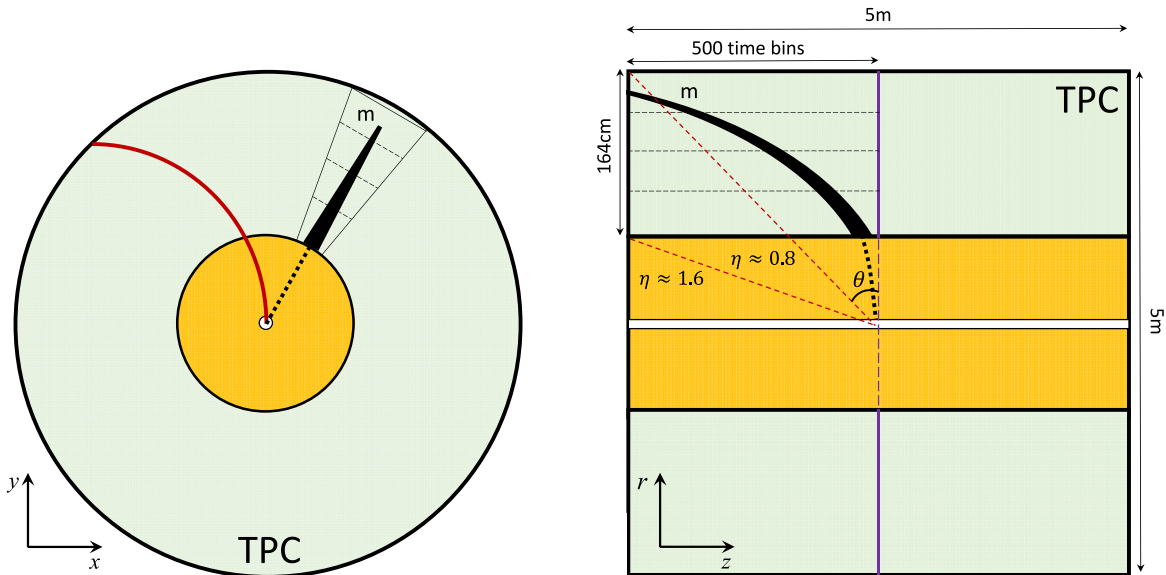


FIG. 4. Left: The $x - y$ ($r - \phi$) projection of the ALICE TPC. The black line denotes a monopole (m) trajectory on a particular TPC sector, its thickness in the green volume labeled “TPC”, indicates the expected energy loss. The red curve represents the helixlike trajectory of a charged particle. Right: The $r - z$ view highlights the parabolic trajectory of the monopole. The black dashed lines represent the segmentation of the four GEM stacks, while the red dashed line at $\eta \approx 0.8$ marks the point where the track length on the $x - y$ plane begins to decrease, continuing until $\eta \approx 1.6$, which represents the border of the geometric acceptance of the TPC. These drawings are simple sketches and are not drawn to scale.

carrying an electric charge with $|z| \approx 68.5$, where z stands for the number of elementary charges in units of “ e ”. Consequently, the ionization caused by a relativistic monopole in matter is expected to exceed the ionization caused by a minimum-ionizing particle (MIP) by more than a factor of 4700. In the presence of a magnetic field, it also exhibits two unique properties. Firstly, it follows a parabolic trajectory [4,39,40], diverging from the anticipated helixlike trajectory of an electrically charged particle moving in a magnetic field. In addition, the energy loss of the monopole decreases as it slows down, whereas an electrically charged particle exhibits the opposite trend, resulting in a Bragg peak when it stops. Both of these characteristics are demonstrated in Fig. 4, which depicts the trajectories of a monopole and a charged particle traversing the gas medium of the ALICE TPC in both the $x - y$ and $r - z$ planes.

Figure 5 compares the energy loss and track length in time bins in the TPC gas between a monopole and a typical high- z particle, in this case, spallation products, which constitute the primary background for the HIP search. The duration for which a monopole track remains in the saturation domain of the readout chip is comparatively longer. Additionally, not only are the characteristics of the energy loss different, but also the magnitude is expected to be relatively larger in the case of monopoles.

Here, it is important to note that monopoles with masses of about 100 GeV are anticipated to be generated through the Schwinger pair production mechanism during

ultraperipheral heavy-ion collisions [41,42]. These collisions are understood to produce the strongest known magnetic fields in the universe, with minimal background interference. In Ref. [17], the MoEDAL Collaboration investigated the production of magnetic monopoles via the Schwinger mechanism in Pb-Pb collisions. They reported a lower mass limit of $75 \text{ GeV}/c^2$ for finite-size magnetic monopoles with Dirac charges of 1, 2, and 3, based on 0.235 nb^{-1} of data collected at 5.02 TeV during the Run 2 data-taking period. The method used by MoEDAL assumes that monopoles are stopped in the magnetic monopole trapper (MMT) detectors requiring them to be within a certain momentum range. This constraint reduces the detection efficiency for monopoles at both very low and very high momentum. In addition, MoEDAL uses nuclear track detectors (NTDs), passive devices consisting of layers of thin plastic sheets. When the NTDs are etched, the damaged areas enlarge to such an extent that they become visible under an optical microscope, revealing the trajectory of the HIPs. In both detection techniques the main source of systematic uncertainty arises from the uncertainty in the material budget, which is estimated to be between 15% and 30% for the default and maximal geometry, respectively. In contrast, ALICE offers two distinct advantages. First, the technique proposed for the ALICE TPC involves continuous tracking of the monopole candidates at any momentum that reaches the TPC, rather than stopping them. This method enables the reconstruction of the full particle trajectory through large sampling points, allowing for both the precise

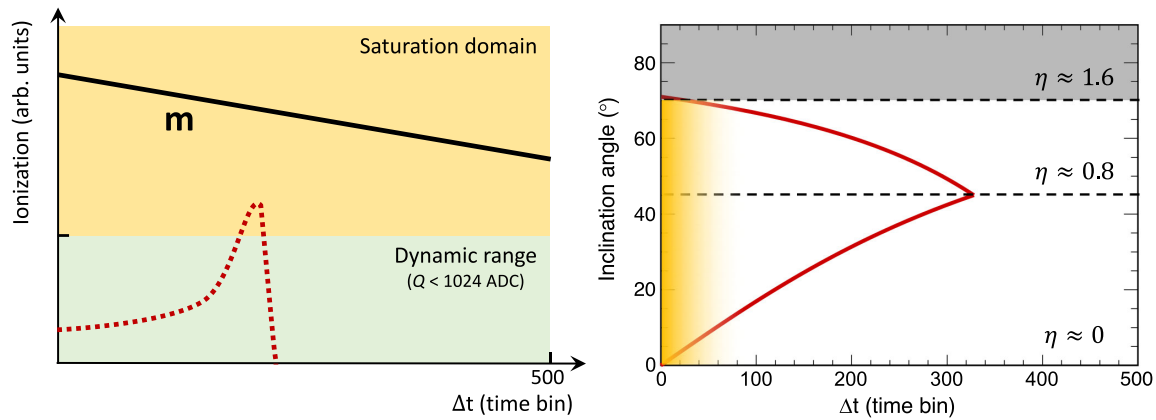


FIG. 5. Left: Expectations of the energy loss over time within the TPC volume for a monopole compared to a typical high- z particle, shown as solid black and dashed red curves, respectively. In the gas, a Bragg peak is observed when the high- z particle stops, while for the monopole the ionization becomes less dense as it loses energy. The green shaded area marks the ionization levels within the dynamic range of the readout electronics where the detected charge per channel remains below 1024 ADC. The yellow area highlights where saturation of the channels occurs. Right: the projection of a HIP track in the saturation domain onto the time (z) axis shown as a function of inclination angle (θ), assuming no bending of the track due to the magnetic field [indeed, monopoles with a large mass ($> \sim 100$ GeV) and low charge would leave a straight track consistent with a very high-momentum electrically charged particle [4]]. Tracks with inclination angles smaller than 45 degrees (i.e., $\eta < 0.8$) exhibit larger Δt values when they bend under the influence of the magnetic field, as depicted in Fig. 4. The gray shaded area shows the angles outside the geometric acceptance of the TPC, while the orange shaded area with a color gradient indicates where the background for the HIPs, mainly spallation products, is anticipated and should be investigated experimentally.

determination of the particle's kinematics and energy loss in the gas. Second, the ALICE detector has a relatively low material budget, which amounts to a radiation thickness of about 11.4% X_0 , measured experimentally with a precision of 2.5% during Run 2 [43]. This value is an average over the pseudorapidity range $|\eta| < 0.9$ and integrated in the radial direction (R) up to 180 cm, which corresponds approximately to the radial center of the TPC. In Run 3, the material budget is estimated to be about 6.2% [37], and it will be further reduced in Run 4. Therefore, ALICE can make a significant contribution to monopole and, more generally, to HIP searches at the LHC during Run 3 and Run 4, where an integrated luminosity of approximately 13 nb^{-1} is expected.

Ultimately, the discovery of a monopole using this new technique demands the identification of a single, very highly ionizing parabolic track with decreasing energy loss along its path. The remaining key question—assuming that the monopole survives the material before it reaches the TPC gas—is whether the TPC and its readout can handle such high energy depositions. We address this question in more detail below.

The signal response of the detector using laser calibration data has been recently published by the ALICE TPC collaboration in Ref. [24]. In Fig. 6 three highly ionizing laser tracks and the corresponding signals of a cluster are depicted. In the following, we examine how these signals can be used to test a monopole scenario. The right panel of Fig. 6 shows that signals that are excessively large saturate the dynamic range of the SAMPA chip [23], such that the

sum of the pedestal value and the measured charge (Q) cannot exceed 1024 ADC. This poses a challenge for accurately measuring the signal amplitude. However, using the measured common-mode signal (shown by the blue dashed curve with the total and maximum charge of $Q_{\text{tot,CM}} = -143$ ADC and $Q_{\text{max,CM}} = -80$ ADC, respectively), which is proportional to the total charge recorded in the stack, one can estimate the mean energy loss for a given cluster (measured as MIP equivalent) with the following equation:

$$Q_{\text{max,Laser}} = \frac{[(Q_{\text{max,CM}} \times N_{\text{pads}}) / N_{\text{rows}}] \times (1/k_{\text{CF}})}{Q_{\text{max,MIP}}}, \quad (1)$$

where

- (i) $Q_{\text{max,CM}} \times N_{\text{pads}}$ is the total maximum charge in IROC,
- (ii) N_{rows} is the normalization factor to obtain the energy loss for a given hit point,
- (iii) k_{CF} is the common-mode fraction factor, which is defined as the ratio of the total negative charge to the total positive charge in a given stack (Table 2 of Ref. [24]),
- (iv) $Q_{\text{max,MIP}}$ is used as the normalization factor to get a MIP equivalent value.

By way of demonstration we substitute into this equation the values for the ALICE IROC, see Table I, and determine a MIP equivalent value of 798 for the laser track in Fig. 6. This is approximately six times lower than the MIP equivalent of 4700 determined above for a monopole.

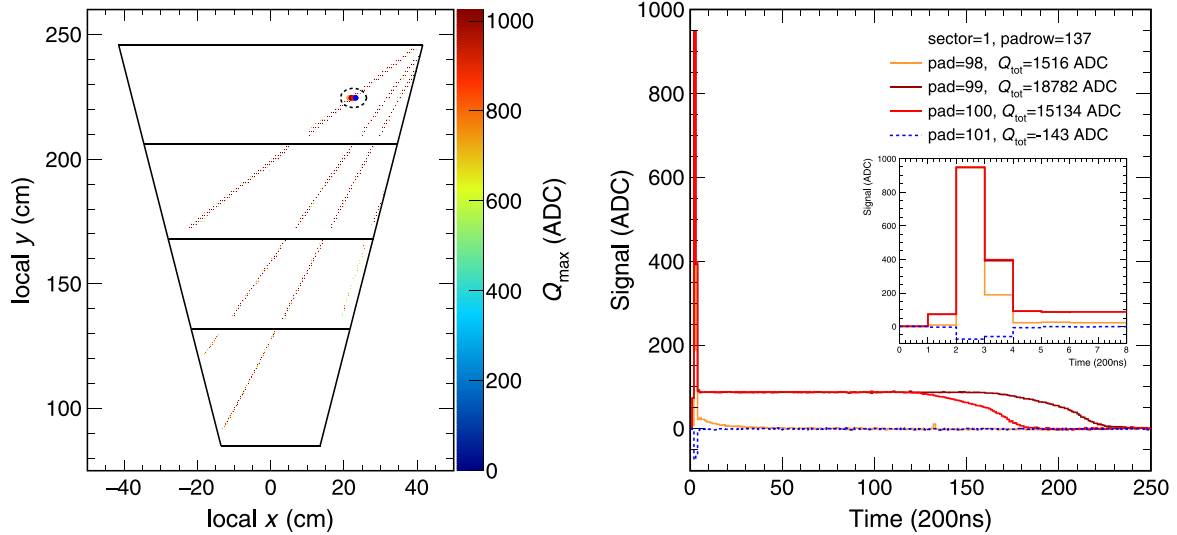


FIG. 6. Left: Three highly ionizing laser tracks in a given TPC readout chamber projected onto the local x - y plane. Radial segmentation of the GEM stacks is also shown with horizontal solid lines ordered from bottom to top: IROC (stack 0), OROC 1 (stack 1), OROC 2 (stack 2), and OROC 3 (stack 3). Right: Saturated signals of a cluster, shown by the dashed circle in the left panel. Note the stable operation of the detector in such high-energy depositions. Figure taken from [24].

It is worth noting that this value applies when the monopole is oriented perpendicular to the beam axis. However, monopoles in a magnetic field are expected to bend along a parabolic trajectory [4,39,40], and thus the deposited charge per monopole cluster is distributed across multiple time bins. More importantly, as illustrated in Fig. 5, the number of time bins, i.e., Δt , for a given monopole track with significant common-mode signals will be comparably large compared to spallation products.

Another important constraint that must be considered is the probability of discharge under conditions of high ionization. This was investigated in Ref. [44], where the reaction of a single GEM setup with gas mixtures based on argon and neon on alpha particles was studied. Discharge occurs when the total accumulated charge within a single GEM hole exceeds the critical charge limit (Q_{crit}). For a Ne-CO₂ (90–10) gas mixture, which can be taken as a reasonable proxy to the original gas mixture of Ne-CO₂-N₂ (90-10-5), Q_{crit} was determined to be $(7.3 \pm 0.9) \times 10^6$ electrons per GEM hole.

To estimate the number of electrons per hole in the IROC geometry [23] for a monopole, one can proceed as follows:

$$N_{\text{el,Mon}} = \frac{[N_{\text{el,MIP}} \times Q_{\text{HIP}} \times k_{\text{gain}}]}{\frac{2\sigma_D}{L_{\text{pitch}}} \times \frac{L_{\text{pad}}}{L_{\text{pitch}}}}, \quad (2)$$

where

- (i) $[N_{\text{el,MIP}} \times Q_{\text{HIP}} \times k_{\text{gain}}]$ is the total number of electrons per pad after gas amplification, the MIP-equivalent energy loss of a monopole is $Q_{\text{HIP}} = 4700$;
- (ii) $2\sigma_D/L_{\text{pitch}}$ accounts for the diffusion of electrons over 5 mm distance ($\sigma_D \approx 2.5$ mm for a flat diffusion assumption in 1 m electron drift);
- (iii) $L_{\text{pad}}/L_{\text{pitch}}$ accounts for the number of holes per pad length.

Using this equation, the calculation yields an electron count per hole of 1.2×10^5 for an ALICE GEM stack, notably one order of magnitude lower than the critical charge, Q_{crit} .

TABLE I. Some ALICE TPC specific variables [23,24].

Variable	Definition	Value
N_{pads}	Number of pads in an IROC	5280
N_{rows}	Number of rows in an IROC	63
k_{CF}	Common-mode fraction factor for an IROC	0.42
$Q_{\text{max,MIP}}$	Mean maximum charge for a MIP signal	20 ADC
k_{gain}	Number of electrons produced per primary electron during gas amplification	2000
$N_{\text{el,MIP}}$	Number of primary electrons per MIP	40
L_{pitch}	Distance between GEM holes	140 μm
L_{pad}	Pad length in IROC	1 cm

In addition with the four-GEM configuration of ALICE, the total gain is distributed among the foils building the stack, resulting in increased stability against discharges. Therefore, this value serves as a conservative lower limit. However, large local charge densities have the potential to trigger sparks that lead to high-voltage trips. Consequently, data acquisition for the chamber is temporarily halted until the high voltage is restored. This interruption begins within a millisecond, while the complete recovery process of the high-voltage power supply takes a few minutes. On the other hand, the signal induction on the pads for the whole track segment occurs on a time scale of less than a microsecond. As a result, even if the signal tail above the baseline is cut off, the common-mode signal below the baseline remains detectable, ensuring that the particle trajectory is measurable.

So far, we have demonstrated the effective performance of GEM-based TPCs in extreme energy loss scenarios. In the following, we outline our systematic proposal for reconstructing the HIP tracks:

- (i) *Hardware trigger in the FPGA*: Two specific pieces of information are required to trigger the monopole candidates: first, for a given pad a high common-mode signal that exceeds a trigger threshold Q_{tr} must be detected. Q_{tr} is set significantly higher than the average baseline shift. Second, a count of subsequent time bins exceeding Q_{tr} (denoted as Δt in Fig. 5) is needed to determine the track length along the z -axis. When Δt is sufficiently large, the pad and time bin of the initiating trigger is flagged to record the signal without baseline subtraction along with the rest of the event data for further analysis. As noted above Δt of a monopole is expected to be significantly larger than that of spallation products and Bragg peaks, allowing effective rejection of background signals. This type of trigger offers two distinct advantages; first, operating at the hardware level enables analysis across any collision system as well as cosmic events. Second, it is sensitive to short track lengths along both the radial and time directions that can not be identified by typical track reconstruction algorithms. Such algorithms struggle to track particles crossing only a few pad rows and usually assume helical trajectories. It is important to emphasize that the parabolic trajectories of low-momentum monopoles are expected to cross only a few pad rows due to their bending along the z -axis, as shown in Fig. 4. Note also that the common-mode signal within a given time bin cannot exceed the pedestal value, which ranges from 40–120 ADC in the ALICE TPC, with an average value of ~ 80 ADC (see Fig. 44 of Ref. [23]), since charge measurements in ADC counts are strictly positive (see Fig. 50 of Ref. [23]). This limitation might complicate the accurate measurement of extreme energy loss cases

where the common-mode signal would exceed the pedestal value. Nevertheless, the particle trajectory and a lower limit of the energy loss via integration of the part of the common-mode signal that is recorded can still be determined.

- (ii) *Raw data recording*: Accurate tracking and energy loss measurement require raw data without subtracting the baseline. The recorded time window must be long enough to cover the entire track candidate ensuring that both the common-mode signals and the signals above the baseline, including long saturation tails, are captured (see blue dashed and solid red curves in Fig. 6, respectively). Note that in the case of MWPCs, i.e., triggered readout, the extended saturation tail would be cut off.
- (iii) *Cluster finding*: Cluster finding algorithm for signals above the baseline should include the entire signal tail for precise energy loss measurement. In the case of a hardware trip, the common-mode signal can still be used as a trigger due to its fast response time, as can the measurement of energy loss, even if the signal tail is distorted.
- (iv) *Tracking*: A special tracking algorithm is required to handle both electrically (helix topology) and magnetically (parabolic topology) charged tracks. This algorithm should be applied to the clusters above the baseline to determine the trajectory, while the measurements of the total charge of these clusters are used together with the common-mode signal to accurately measure the energy loss. This step is particularly important to reject background using the track topology and length information.

In an optimal detector configuration, the measurement of common-mode signals and thus the detection of HIPs can be improved by fine-tuning experimentally adjustable parameters. These parameters include k_{gain} (the multiplication factor of the primary ionization, adjustable through voltage settings on the GEM foils), N_{pads} (proportional to the capacitance, i.e., GEM stack area facing the pad plane), the number of layers, the distance to the collision point, the magnetic field strength, the material budget before the TPC, the dynamic range of the readout chips and the pedestal values of the readout channels.

Accordingly, the recipe for the ideal TPC for HIP detection is summarized as follows. The k_{gain} parameter should be set low, e.g., to 100 instead of 2000, to increase the sensitivity to HIPs while suppressing signals from all other standard-model particle species including electrons, muons, pions, kaons, protons, etc.. By significantly reducing the recorded track density this adjustment would also help mitigate the space charge generated in the amplification region. Such conditions would be suitable for any TPC designed for HIP detection across various interaction rate scenarios.

By optimizing the high-voltage segmentation of the GEM foils, the capacitance between the pad plane and the GEM stack can be adjusted to ensure that the common-mode signal does not exceed the pedestal. Additionally, increasing the number of GEM layers would enhance stability against discharge [44]. Minimizing the material budget, which involves avoiding additional detectors before the TPC and reducing the material budget for the beam pipe, will maximize the probability that the monopole survives and enters the active volume of the TPC. This prevents the HIPs from stopping before reaching the TPC and also reduces the distance between the TPC and the beam pipe, thereby enhancing the kinematic acceptance. For example, one could consider utilizing the geometry of the yellow area instead of the green in Fig. 4, which enables a more compact TPC design with a geometric coverage close to 4π due to the minimal distance to the collision point. Moreover, increasing the magnetic field to 2 T instead of 0.5 T would increase track bending and thus increase the track length along the z -axis, i.e., the number of common-mode triggers. Expanding the dynamic range of the readout chip beyond 1024 ADC enables the measurement of larger energy depositions. Finally, setting a high pedestal value, e.g., 1000 ADC, will increase the dynamic range of the HIP's common-mode signal thereby facilitating precise energy-loss measurements.

IV. CONCLUSIONS

This article presents a new approach utilizing time projection chambers to detect highly ionizing particles such as monopoles. As an illustration, we examined the response of the ALICE TPC to energy depositions corresponding to those of a Dirac monopole, equivalent to 4700 MIPs. Our findings indicate that the measured signals, corresponding to an energy loss of about 798 MIPs, are promising to achieve this goal. Additionally, we have estimated the number of electrons per hole under the

conditions of 4700 MIPs and found it to be about an order of magnitude below the critical charge density, where discharges occur. Moreover, we investigated the possibility that in cases where detector stability is compromised, reconstruction of the common-mode signal remains a viable option for tracking and measuring the energy loss of the highly-ionizing particles.

After validating the stable operation of the GEM-based ALICE TPC under significant energy depositions, we have introduced an innovative method in which the TPC functions as a passive detector. This method utilizes the negatively polarized common-mode signal as a hardware trigger in the readout electronics, enabling the recording of digitized raw data without loss of information, which is crucial for precise energy loss and mass measurements. We then elaborated on a TPC-based detector design that, in combination with this technique, can serve as an optimal detector offering complete 4π coverage for the study of highly ionizing particles beyond the Standard Model. Such a detector is well suited for both high and low interaction rate scenarios and offers significant advantages in the discovery of HIPs, in particular monopoles in background-free ultraperipheral heavy ion collisions.

ACKNOWLEDGMENTS

We would like to thank Chilo Garabatos, Robert Helmut Münzer, and Christian Lippmann for their valuable discussions regarding the ALICE TPC and its stability, and to Torsten Alt, Peter Hristov, David Rohr, and Ruben Shahoyan for their insights on the data acquisition system of the ALICE detector. This work is supported in part by the U.S. Department of Energy, Office of Science, Office of Nuclear Physics under grant Contract No. DE-SC0004168, the Bundesministerium für Bildung und Forschung (BMBF) and GSI Helmholtzzentrum für Schwerionenforschung GmbH, Germany.

-
- [1] P. Nath *et al.*, The hunt for new physics at the large hadron collider, *Nucl. Phys. B, Proc. Suppl.* **200–202**, 185 (2010).
 - [2] W. M. Yao *et al.* (Particle Data Group), Review of particle physics, *J. Phys. G* **33**, 1 (2006).
 - [3] M. L. Perl, P. C. Kim, V. Halyo, E. R. Lee, I. T. Lee, D. Loomba, and K. S. Lackner, The search for stable, massive, elementary particles, *Int. J. Mod. Phys. A* **16**, 2137 (2001).
 - [4] M. Fairbairn, A. C. Kraan, D. A. Milstead, T. Sjostrand, P. Z. Skands, and T. Sloan, Stable massive particles at colliders, *Phys. Rep.* **438**, 1 (2007).
 - [5] N. E. Mavromatos and V. A. Mitsou, Magnetic monopoles revisited: Models and searches at colliders and in the Cosmos, *Int. J. Mod. Phys. A* **35**, 2030012 (2020).
 - [6] G. 't Hooft, Magnetic monopoles in unified gauge theories, *Nucl. Phys.* **B79**, 276 (1974).
 - [7] J. Alimena *et al.*, Searching for long-lived particles beyond the Standard Model at the Large Hadron Collider, *J. Phys. G* **47**, 090501 (2020).
 - [8] G. Aad *et al.* (ATLAS Collaboration), Search for magnetic monopoles and stable particles with high electric charges in 8 TeV pp collisions with the ATLAS detector, *Phys. Rev. D* **93**, 052009 (2016).

- [9] G. Aad *et al.* (ATLAS Collaboration), Search for magnetic monopoles in $\sqrt{s} = 7$ TeV pp collisions with the ATLAS detector, *Phys. Rev. Lett.* **109**, 261803 (2012).
- [10] G. Aad *et al.* (ATLAS Collaboration), Search for magnetic monopoles and stable particles with high electric charges in $\sqrt{s} = 13$ TeV pp collisions with the ATLAS detector, *J. High Energy Phys.* **11** (2023) 112.
- [11] M. M. Hassan El Sawy, Search for magnetic monopoles in the CMS experiment at the Large Hadron Collider (LHC), Ph.D. thesis, Antwerp U., 2020.
- [12] B. Acharya *et al.* (MoEDAL Collaboration), The physics programme of the MoEDAL experiment at the LHC, *Int. J. Mod. Phys. A* **29**, 1430050 (2014).
- [13] B. Acharya *et al.* (MoEDAL Collaboration), Search for magnetic monopoles with the MoEDAL prototype trapping detector in 8 TeV proton-proton collisions at the LHC, *J. High Energy Phys.* **08** (2016) 067.
- [14] B. Acharya *et al.* (MoEDAL Collaboration), Search for magnetic monopoles with the MoEDAL forward trapping detector in 13 TeV proton-proton collisions at the LHC, *Phys. Rev. Lett.* **118**, 061801 (2017).
- [15] B. Acharya *et al.* (MoEDAL Collaboration), Search for magnetic monopoles with the MoEDAL forward trapping detector in 2.11 fb^{-1} of 13 TeV proton-proton collisions at the LHC, *Phys. Lett. B* **782**, 510 (2018).
- [16] B. Acharya *et al.* (MoEDAL Collaboration), Magnetic monopole search with the full MoEDAL trapping detector in 13 TeV pp collisions interpreted in photon-fusion and Drell-Yan production, *Phys. Rev. Lett.* **123**, 021802 (2019).
- [17] B. Acharya *et al.* (MoEDAL Collaboration), Search for magnetic monopoles produced via the Schwinger mechanism, *Nature (London)* **602**, 63 (2022).
- [18] V. A. Mitsou (MoEDAL Collaboration), First search for magnetic monopoles through the Schwinger mechanism, *J. Phys. Conf. Ser.* **2375**, 012002 (2022).
- [19] W. Adam *et al.* (CMS Tracker Collaboration), The effect of highly ionising particles on the CMS silicon strip tracker, *Nucl. Instrum. Methods Phys. Res., Sect. A* **543**, 463 (2005).
- [20] R. Barate *et al.* (ALEPH Collaboration), Search for pair production of long-lived heavy charged particles in e^+e^- annihilation, *Phys. Lett. B* **405**, 379 (1997).
- [21] F. Sauli, GEM: A new concept for electron amplification in gas detectors, *Nucl. Instrum. Methods Phys. Res., Sect. A* **386**, 531 (1997).
- [22] F. Sauli, *Gaseous Radiation Detectors: Fundamentals and Applications* (Oxford University Press, New York, 2015), Vol. 36.
- [23] J. Adolfsson *et al.* (ALICE TPC Collaboration), The upgrade of the ALICE TPC with GEMs and continuous readout, *J. Instrum.* **16**, P03022 (2021).
- [24] J. Alme *et al.* (ALICE TPC Collaboration), Correction of the baseline fluctuations in the GEM-based ALICE TPC, *J. Instrum.* **18**, P11021 (2023).
- [25] K. Aamodt *et al.* (ALICE Collaboration), The ALICE experiment at the CERN LHC, *J. Instrum.* **3**, S08002 (2008).
- [26] B. B. Abelev *et al.* (ALICE Collaboration), Performance of the ALICE experiment at the CERN LHC, *Int. J. Mod. Phys. A* **29**, 1430044 (2014).
- [27] J. N. Marx and D. R. Nygren, The Time Projection Chamber, *Phys. Today* **31**, 10, 46 (1974).
- [28] D. R. Nygren, TPC workshop summary, *AIP Conf. Proc.* **108**, 262 (1984).
- [29] G. Charpak, F. Sauli, and W. Duinker, High-accuracy drift chambers and their use in strong magnetic fields, *Nucl. Instrum. Methods* **108**, 413 (1973).
- [30] N. Abgrall *et al.* (NA61 Collaboration), NA61/SHINE facility at the CERN SPS: Beams and detector system, *J. Instrum.* **9**, P06005 (2014).
- [31] H. Wieman *et al.* (STAR Collaboration), STAR TPC at RHIC, *IEEE Trans. Nucl. Sci.* **44**, 671 (1997).
- [32] M. E. Beddo *et al.* (STAR Collaboration), STAR: Conceptual design report for the Solenoidal tracker at RHIC, BNL-PUB-5347, 1992.
- [33] H. T. Klest (sPHENIX Collaboration), A compact TPC for the sPHENIX experiment, *J. Phys. Conf. Ser.* **2374**, 012147 (2022).
- [34] J. Alme *et al.* (ALICE TPC Collaboration), The ALICE TPC, a large 3-dimensional tracking device with fast readout for ultra-high multiplicity events, *Nucl. Instrum. Methods Phys. Res., Sect. A* **622**, 316 (2010).
- [35] G. Dellacasa *et al.* (ALICE Collaboration), ALICE: Technical design report of the time projection chamber, Report No. CERN-OPEN-2000-183, CERN-LHCC-2000-001, 2000.
- [36] Upgrade of the ALICE time projection chamber, Technical Report No. CERN-LHCC-2013-020, ALICE-TDR-16, CERN, 2013.
- [37] B. Abelev *et al.* (ALICE Collaboration), Upgrade of the ALICE experiment: Letter of intent, *J. Phys. G* **41**, 087001 (2014).
- [38] M. Arslandok, Event-by-event identified particle ratio fluctuations in Pb–Pb collisions with ALICE, Ph.D. thesis, Frankfurt U., 2017, presented 04 Dec 2017.
- [39] W. Braunschweig *et al.* (TASSO Collaboration), A search for particles with magnetic charge produced in e^+e^- annihilations at $\sqrt{s} = 35$ -GeV, *Z. Phys. C* **38**, 543 (1988).
- [40] G. Bauer, M. J. Mulhearn, C. Paus, P. Schieferdecker, and S. Tether, Simulating magnetic monopoles by extending GEANT, *Nucl. Instrum. Methods Phys. Res., Sect. A* **545**, 503 (2005).
- [41] O. Gould, D. L. J. Ho, and A. Rajantie, Towards Schwinger production of magnetic monopoles in heavy-ion collisions, *Phys. Rev. D* **100**, 015041 (2019).
- [42] O. Gould, D. L. J. Ho, and A. Rajantie, Schwinger pair production of magnetic monopoles: Momentum distribution for heavy-ion collisions, *Phys. Rev. D* **104**, 015033 (2021).
- [43] S. Acharya *et al.* (ALICE Collaboration), Data-driven precision determination of the material budget in ALICE, *J. Instrum.* **18**, P11032 (2023).
- [44] P. Gasik, A. Mathis, L. Fabbietti, and J. Margutti, Charge density as a driving factor of discharge formation in GEM-based detectors, *Nucl. Instrum. Methods Phys. Res., Sect. A* **870**, 116 (2017).